Urban Rail Substation Parameter Optimization by Energy Audit and Modified Salp Swarm Algorithm

Jian Zhang, Wei Liu, Zhongbei Tian, He Qi, Jiaxin Zeng, Yuheng Yang

***Abstract*-- Auditing the energy consumption in urban rail is vital for energy consumption evaluation and system parameter design. There are multiple ways to audit energy consumption, but a universal and global approach is missing. The system-level traction energy consumption (STEC) is proposed. Compared to the main substation energy consumption (MSEC), STEC is more accurate by eliminating the influence of step-down loads based on field test studies. An optimization parameter designing model is built, which takes the system cost as the optimal object considering the life span of energy feedback system (EFS)s. The modified salp swarm algorithm (MSSA) is proposed as the optimization algorithm. The numerical tests show that MSSA has better converge performance than salp swarm algorithm (SSA) and particle swarm optimization (PSO). The impact factors of STEC are analyzed. Compared with SSA and PSO, the initial value of the MSSA is improved and it evolves faster. Compared with the case that does not take the no-load voltage of rectifiers and start voltage of EFSs as optimal parameters, the composite cost of the case that takes the abovementioned parameters as optimal parameters is 3.49% less. Compared to the system without EFSs, the optimal system with EFSs can save costs by 29.47%.**

***Index Terms*—Energy audit; Modified salp swarm algorithm; Optimization parameter designing**

NOMENCLATURE

Symbol	Definition
U_s	The starting voltage of the energy feedback system (EFS) [V]
U_0	The no-load voltage of the rectifier unit [V]
W_M	Active energy of all main transformers in contradistinction system (CS) [kWh]
W_T	The total active energy of all rectifier units in CS [kWh]
W_F	Feedback energy of all energy feedback system (EFS)s at the AC side in CS [kWh]
W_R	Energy returned to the main substation (MS)s in CS [kWh]
$W_{reg\text{-}trac}$	Regenerative braking energy absorbed by the adjacent trains in CS [kWh]
W_{res}	Total energy consumed by on-board braking resistors in CS [kWh]
W_{loss1}	Energy dissipated on DC traction network (TN) between braking trains and traction trains in CS [kWh]
W_{loss2}	Energy dissipated on DC TN between rectifiers and traction trains in CS [kWh]
W_M'	Active energy of all main transformers in reference system (RS) [kWh]
W_T'	The total active energy of all rectifier units in RS [kWh]
$W_{reg\text{-}trac}'$	Regenerative braking energy absorbed by the adjacent trains in RS [kWh]
W_{res}'	Total energy consumed by on-board braking resistors in RS [kWh]
W_{loss1}'	Energy dissipated on DC TN between braking trains and traction trains in RS [kWh]
W_{loss2}'	Energy dissipated on DC TN between rectifiers and traction trains in RS [kWh]
W_S	The active energy of step-down loads [kWh]
W_{trac}	Total energy consumption of tracting trains [kWh]
W_{reg}	The total regenerative braking energy of braking trains [kWh]
η_T	The efficiency of the rectifier unit
η_F	The efficiency of the EFS
W_{TR}	System-level traction energy consumption (STEC) in CS [kWh]
W_{TR}'	STEC in RS [kWh]
S	The rated power of EFS [kW]
$\mathbf{S}$	The collection of S
$\boldsymbol{U_s}$	The collection of U_s
$F(\mathbf{S}, U_0, \boldsymbol{U_s})$	Optimization objective
$f_1(\mathbf{S})$, $f_2(\mathbf{S},U_0,\boldsymbol{U_s})$	Sub-objective functions

This work was supported in part by the National Natural Science Foundation of China (Grant Nos. 51607148) and China Scholarship Council. The corresponding authors are Wei Liu and Zhongbei Tian.

Jian Zhang is with the School of Electrical Engineering, Southwest Jiaotong University, Chengdu, China (e-mail: zhangjian95@foxmail.com).

Wei Liu is with the School of Electrical Engineering, Southwest Jiaotong University, Chengdu, China (e-mail: liuwei_8208@swjtu.cn).

Zhongbei Tian is with the Department of Electrical Engineering and Electronics, University of Liverpool, Liverpool, U.K. (e-mail: Zhongbei.tian@liverpool.ac.uk).

He Qi is with the School of Electrical Engineering, Southwest Jiaotong University, Chengdu, China (e-mail: zy728734777@163.com).

Jiaxin Zeng is with the School of Electrical Engineering, Southwest Jiaotong University, Chengdu, China (e-mail: zjx9805@163.com).

Yuheng Yang is with the School of Electrical Engineering, Southwest Jiaotong University, Chengdu, China (e-mail: yyh838766021@my.swjtu.edu.cn).

U_{si}	Start voltage of EFS in the *i*-th traction substation (TS) [V]
ε_{S}	Feasible region of **S**
$\varepsilon_{\mathrm{U_0}}$	Feasible region of U_0
$\varepsilon_{\mathrm{U_s}}$	Feasible region of $\mathbf{U_s}$
y	The number of years since the installation of the EFSs
U_{rmax}	Maximum allowable value of the rail potential
U_{t}	TN voltage
U_{tmax}	Maximum allowable value of the TN voltage
U_{tmin}	Minimum allowable value of the TN voltage

I. Introduction

THE urban rail power supply system includes regenerative braking energy utilization devices, such as the EFS, energy storage system (ESS) [1] and bidirectional converter device [2]. Since there is no unified and standard method to evaluate the energy-saving effect of EFSs, it is common for EFS manufacturers to evaluate the energy-saving effect by the ratio of the feedback energy and the rectifying energy of a single TS. However, auditing energy at a specific substation cannot reflect the energy consumption level of the power supply system. An index that considers the system-level energy consumption is needed. As for the parameter designing of EFS, the system-level energy-saving effect and the composite cost of the system need to be considered. When calculating the composite cost of the system, the life span of EFSs, the inflation, and the multiple train operation timetables during the life span should be considered. Till now, the parameter designing methods include the expert empirical method and artificial intelligence (AI) algorithm. AI algorithm has advantages such as high efficiency and strong global search capability. However, with the development of AI algorithms nowadays, there is still space for algorithms to improve and evolve. In this paper, only the urban rail system with EFSs are discussed.

In terms of urban rail energy consumption, Tian introduces the conception “Energy audit” [3]. The energy audit is to reflect the system energy consumption level, and the energy supplied by the substations is calculated. In [3], the traction energy, braking energy, RBE, substation energy, and energy loss are calculated. [4]-[6] audit energy from the aspect of traction substation. The system energy consumption is ignored. [7] audits energy from the aspect of trains. In [8], the system-level energy consumption is analyzed. However, the power flow structure of the high speed railway is different from the structure of urban rail. In [9], the energy audit index is the main substation energy consumption (MSEC), and the system-level energy-saving effect is effectively performed. But the index is not verified by the actual cases. In [10]-[11], various global substation energy consumption methods are proposed, but the reversed energy in main substations is neglected, which also affects the energy audit. The above research does not consider EFSs or does not consider reverse energy at main stations. Therefore, a reasonable and global energy audit index is needed for energy consumption evaluation and system parameter designing, but it needs to be studied further. In this paper, only urban rail system with EFSs are discussed.

The parameter designing is closely related with the energy audit index. As for parameter designing of system with EFSs, the target is achieving high return on investment (ROI) as well as energy-saving effect. To improve the efficiency of system parameter designing, Lian uses the genetic algorithm (GA) to optimize the EFS rated power. However, the difference in the rated power of the EFS before and after optimization was less than 0.2 MW [14]. Wlodzimierz takes ROI as the final optimization aim, but the rated power of EFS should not be continuous values [15]. In [18], to minimize system energy consumption in the life span of EFS, particle swarm optimization (PSO) is used to obtain the location and rated power optimization solution of EFS. However, the starting voltage is not considered, which influences the energy-saving effect of EFSs directly.

Salp Swarm Algorithm (SSA) [19] has been widely used since it was proposed in 2017. The algorithm simulates the behavior of salps and adopts a chain structure. It has only one main control parameter, so it is simple to implement [16]-[17]. However, SSA has defects such as easily falling into local optimum, low optimization accuracy, and slow convergence speed. The "No-Free-Lunch" theorem indicates that no algorithm can be applied to all optimization problems [20]. To obtain better results, [21]-[23] introduce adaptive parameters to accelerate evolution. In [21] and [24], the chaotic map is introduced to optimize the population initialization process. In [25] and [26], the spiral flight search (SFS) strategy and Levy flight strategy are introduced and have a positive effect on the evolution process. Other strategies, including hybrid locomotion [27], PSO [28], quantum-behaved and wavelet mutation[29], opposition-based learning [30] can also accelerate evolution speed. There are no cases which apply the SSA algorithm in urban rail design, not to mention the improved SSA algorithm. For SSA algorithm, it has room for improvement in areas such as population initialization, population selection, and random variation disturbance.

The main contributions of this paper can be summarized as follows:

1) An energy audit index, which is system-level energy consumption (STEC), is proposed. It counts energy from the system level. It is proved to be more effective than MSEC and can avoid the fluctuation of step-down loads through the field test. Therefore, it can be widely used in urban rail system with EFSs.

2) The optimization parameter designing model of the system with EFSs is built. The composite cost is the optimal object. The install and maintenance cost of EFSs, the life span of EFSs, the inflation, and the multiple train operation timetables during the life span are considered.

3) The modified SSA (MSSA) is proposed, which introduces Tent chaotic mapping, global adaptive inertia weight, and differential mutation algorithm. Numerical tests show that it has better performance than PSO and SSA.

4) The case study shows that by using MSSA, the composite cost can save 29.47% 1.43%, and 3.50% compared to the reference system without EFSs, PSO, SSA respectively.

5) The influence of U_0 and U_s is analyzed in the case studies.

The composite cost of MSSA without U_0 and U_s is 3.49% more than the composite cost of MSSA with U_0 and U_s. It can be shown that U_0 and U_s should be taken into account when designing the parameters. It can guide the subway design institutions on system designing.

This paper is organized as follows: Section II first analyzes the energy flow in the power supply system in urban rail; then the energy audit index is proposed; the rationality of STEC is verified through the field test data. In section III, the parameter designing model is proposed, which aims to minimize the composite cost of the system when EFSs reach their life span. In section IV, PSO and SSA are introduced, and the MSSA is proposed. In section V, numerical tests are carried out and the performance of PSO, SSA, and MSSA is compared. In section VI, the influence of U_0 and U_s is first analyzed in the case. Then the results of RS, PSO, SSA, MSSA with rated power as the optimization parameter and MSSA with all parameters of parameter designing model as optimization parameters are analyzed.

II. Energy Audit and Parameter Designing Model

In the urban rail of China, the structure of the power supply system contains main substation (MS)s, traction substation (TS)s, step-down substation (SS)s. The most applied structure of power supply system is: MSs transfer AC 110kV to AC 35 kV and connect the AC 35 kV buses. The buses then connect to the TSs and SSs. In TSs, the rectifiers convert AC 35kV to DC 1500V and are connected to DC 1500V buses. The buses connect to the traction network (TN), the rail, and the EFSs. EFSs can feed energy from the DC bus to AC 35 kV side. The step-down loads obtain energy from step-down transformers. In SSs, there are only step-down loads. The step-down loads include lighting, air conditioning system, electric lifts, and so on.

It is worth mentioning that U_0 should be lower than U_s to avoid the rectifier and EFS working together, or the efficiency of the power supply system will decrease. U_s can be set manually and change automatically with the voltage fluctuation on the AC side.

Energy audit can reflect the system energy consumption level [3]. To evaluate energy consumption and design system parameter, a reasonable index of energy audit is necessary.

A. Energy audit index

The energy audit can be implemented at main substation (MS)s or TSs. To compare these two methods, the power supply system without EFSs is defined as the reference system (RS). Correspondingly, the power supply system with EFS installed is defined as the contradistinction system (CS).

The schematic diagram of the energy flow of RS is shown in Fig. 1. The energy of MSs (W_M') has 2 flow directions: rectifier units (W_T') and step-down loads (W_S'). The energy from rectifies units is $\eta_T W_T'$. After the loss of traction network(W_{loss2}'), the $\eta_T W_T'$ will flow to tracting trains. Besides, tracting trains will also receive energy from braking trains($W_{reg\text{-}trac}'$). After supplying the kinetic energy, auxiliary energy consumption and power loss of trains, the remaining energy is W_{reg}. W_{reg} has 2 flow directions: the on-board braking resistors(W_{res}') and tracting trains($W_{reg\text{-}trac}'$). The loss during the process is W_{loss2}'. The energy loss on the AC cables is ignored.

Based on Fig. 1., the relationship between system energy in RS is shown as (1).

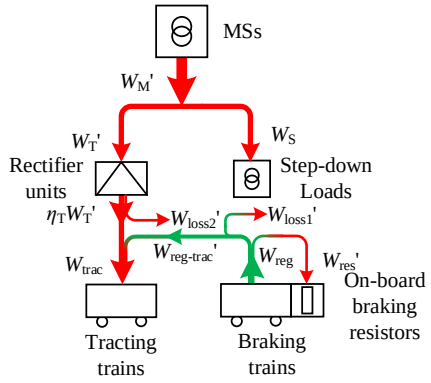

Fig. 1. Schematic diagram of energy flow of RS.

$$\begin{cases} W_M' = W_T' + W_S \\ W_{trac} = \eta_T W_T' + W_{reg\text{-}trac}' - W_{loss2}' \\ W_{reg} = W_{res}' + W_{reg\text{-}trac}' + W_{loss1}' \end{cases} \quad (1)$$

The schematic diagram of the energy flow of CS is shown in Fig. 2. Compared with Fig. 1, W_{reg} has a more flow direction: EFS (W_F/η_F). This part of energy will flow to rectifier units, step-down loads, and MSs (W_R).

The relationship between system energy in CS is shown as (2). The energy loss on the cables is ignored.

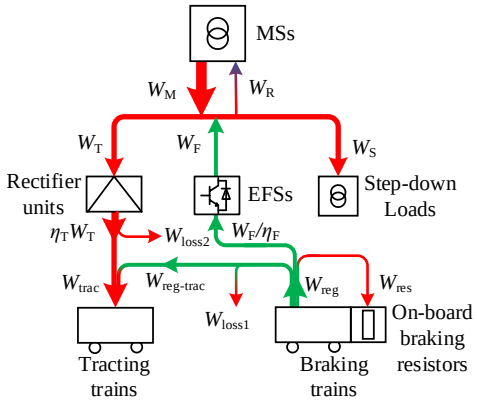

Fig. 2. Schematic diagram of energy flow of CS

$$\begin{cases} W_M = W_T - W_F + W_S + W_R \\ W_{trac} = \eta_T W_T + W_{reg\text{-}trac} - W_{loss2} \\ W_{reg} = W_F / \eta_F + W_{res} + W_{reg\text{-}trac} + W_{loss1} \end{cases} \quad (2)$$

When the MSEC is the index of energy audit, W_M and W_M' are the energy consumption values of CS and RS. The difference between the energy consumption of CS and RS is the energy saving of CS [1].

When the STEC is the index of energy audit, W_{TR} and W_{TR}' are the energy consumption values of CS and RS. In CS, W_{TR} is shown in (3). In RS, W_{TR}' is W_T'. The difference between W_{TR}' and W_{TR} is the energy saving of CS.

$$W_{TR} = W_M - W_S = W_T - W_F + W_R \quad (3)$$

B. Comparison of MSEC and STEC

Compared with simulation data, field test data is closer to real data. To compare the performance of MSEC and STEC, a field test is carried out in a subway of Shenzhen. In this subway line, there are 1 MS, 6 TSs, and 3 step-down substation (SS)s. The topology is shown in Fig. 3. EFSs are set at TS④, TS⑤, TS⑦, TS⑧, and TS⑨, with the rated power of 2MW. The substation positions are shown in TABLE I. The train is composed of 6 sections, with the highest speed limit of 80km/h and the weight of 328.6t. The energy consumption of the main station and the traction energy consumption of all TSs were monitored. The monitor period for CS and RS is 7 days.

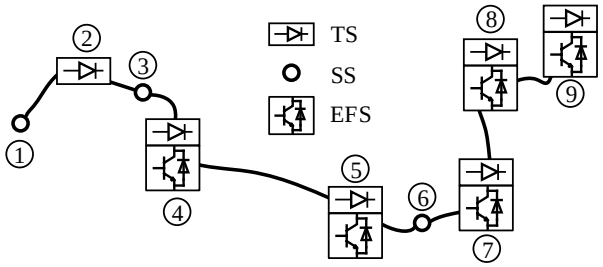

Fig. 3. Topology of the subway in Shenzhen.

TABLE I
SUBSTATION POSITIONS OF THE SUBWAY IN SHENZHEN

Station	Position (km)	Station	Position (km)
①	0.697	⑥	10.797
②	2.642	⑦	11.593
③	3.442	⑧	14.577
④	4.883	⑨	15.942
⑤	9.194		

Fig. 4. shows the energy consumption in CS (Day1~7) and RS (Day8~14). Day 2, 3, 9, and 10 are weekend days, and other days are workdays. In Fig. 4., to distinguish between the step-down loads in CS and the step-down loads in RS, W_S' is the step-down loads in RS, and W_S is the step-down loads in CS. W_S and W_S' are calculated from (1) to (3).

In CS, the difference between the maximum W_{TR} and minimum W_{TR} is 13, 052 kWh. The difference between the maximum W_S and minimum W_S is 22, 383 kWh. In RS, the difference between the maximum W_{TR}' and minimum W_{TR}' is 8, 034 kWh. The difference between the maximum W_S' and minimum W_S' is 46, 311 kWh. The fluctuation of step-down loads is greater than the fluctuation of STEC, causing the MSEC to have a wild fluctuation. Applying STEC can avoid the influence of fluctuation of step-down loads. Therefore, STEC, rather than MSEC, should be the energy audit index. It is also worth mentioning that utilizing STEC needs the data of all TSs and MSs. If there are data collecting system in the subway project, it will be easy to collect the data. And it takes short time to collect data in simulation results.

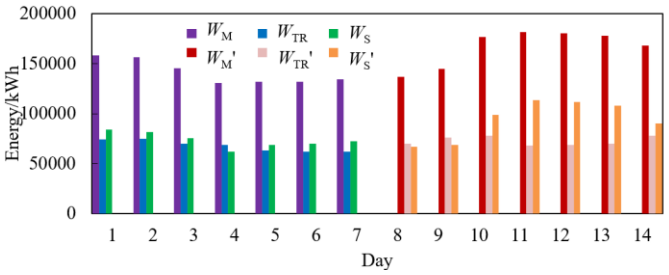

Fig. 4. Energy consumption in CS and RS.

C. Parameter designing model

Taking into account the life span of EFSs, from the perspective of the economics of the power supply system, the overall cost of the system should be calculated when the life span of the EFS is reached. The parameter designing model is:

$$\min \quad F(\mathbf{S},U_0,\mathbf{U_s}) = f_1(\mathbf{S})+f_2(\mathbf{S},U_0,\mathbf{U_s})$$
$$s.t.\begin{cases}\mathbf{S}\in\varepsilon_S\\ U_0\in\varepsilon_{U_0}\\ \mathbf{U_s}\in\varepsilon_{U_s}\end{cases} \tag{4}$$

where $F(\mathbf{S}, U_0, \mathbf{U_S})$ is the optimization objective. It is the comprehensive cost of the system when the EFS life span is reached. It is composed of sub-objective functions $f_1(\mathbf{S})$ and $f_2(\mathbf{S},U_0,\mathbf{U_S})$; $\mathbf{S}=\{S_i \mid i=1,2\cdots N\}$. S_i is the rated power of the EFS in the i-th TS. N is the number of TSs. U_0 is the no-load voltage of the rectifier units. $\mathbf{U_S}=\{U_{si} \mid i=1,2\cdots N\}$. U_{si} is the start voltage of EFS in the i-th TS. ε_S, ε_{U_0} and ε_{U_s} are the feasible region of $\mathbf{S}$, U_0, and $\mathbf{U_S}$.

The sub-objective function $f_1(\mathbf{S})$ is the total cost of the system when the life span of EFSs is reached. It is:

$$f_1(\mathbf{S}) = \sum_{i=1}^{N} c_{ins}(S_i)r^y + \sum_{y=1}^{Y}\sum_{i=1}^{N} c_{mt}(S_i)r^y \tag{5}$$

where $c_{ins}(S_i)$ is the cost of installing the EFS in the i-th TS with the rated power of S_i. $c_{mt}(S_i)$ is the annual cost of maintaining the EFS in the i-th TS with the rated power of S_i. r is the currency inflation coefficient. y is the year from the installation of the EFSs. Y is the EFS life span in years.

EFS installation cost $c_{ins}(S)$ is:

$$c_{ins}(S) = c_0 + p_c S \tag{6}$$

where c_0 is the fixed cost, which is 700,000 RMB. p_c is the unit rated power cost, which is 400,000 RMB/MW. $\varepsilon_S=\{0.5x \mid x=0,1,2,3,4,5,6\}$ (MW).

The sub-objective function $f_2(\mathbf{S}, U_0, \mathbf{U_S})$ is the total traction electricity cost when the EFS life span is reached. It is:

$$f_2(\mathbf{S},U_0,\mathbf{U_s}) = \sum_{y=1}^{Y} W_{TRy}(\mathbf{S},U_0,\mathbf{U_s})E_y r^y \tag{7}$$

where $W_{TRy}(\mathbf{S}, U_0, \mathbf{U_S})$ is the actual traction energy consumption of the whole line in the y-th year corresponding to the configuration of $\mathbf{S}$, U_0, $\mathbf{U_S}$. E_y is the electricity price in the y-th year.

Constraints include TN voltage, rail potential, and no-load voltage. They are:

$$\begin{cases} |U_{\mathrm{r}}| \leqslant U_{\mathrm{rmax}} \\ U_{\mathrm{tmin}} \leqslant U_{\mathrm{t}} \leqslant U_{\mathrm{tmax}} \\ U_{\mathrm{d0}} \leqslant U_{\mathrm{s}} \end{cases} \tag{8}$$

where U_{r} is the rail potential.

III. Optimization Algorithms

In this section, three optimization algorithms are introduced and compared numerical tests.

Particle Swarm Optimization (PSO) uses particle simulation to achieve the optimization goal. Salp Swarm Algorithm (SSA) is an intelligent optimization Algorithm for simulating salp organisms. MSSA is first proposed in this paper. It introduces Tent chaotic mapping, global adaptive inertia weight, and differential mutation algorithm, and will be illustrated in part C of this Section.

Both PSO and SSA take population as the basic unit for optimization, so there are similarities in the definition as below: The population $\mathbf{X}$ is a collection of individual $\boldsymbol{x^i}$, namely $\mathbf{X} = \{\boldsymbol{x^i} \mid i=1,2 \cdots N\}$. N is the number of individuals in the population. The individual is defined as $\boldsymbol{x^i}=(x^i_1\, x^i_2, \cdots, x^i_D)$. x^i_j is the variable on the j-th dimension. D is the number of dimensions. t is defined as the number of iterations. $x^i_j(t)$ is the variable on the j-th dimension of individual $\boldsymbol{x^i}$ at the t-th iteration. Individuals have upper limit ***ub*** and lower limit ***lb***. The dimensions of ***ub*** and ***lb*** are consistent with individuals. The value of the individual is defined as the position of the individual. The objective function value of the individual is defined as the fitness of the individual.

A. PSO

In the PSO algorithm, in addition to the location, the variables of the individual also include the velocity, $\boldsymbol{V^i}= (V^i_1, V^i_2, \cdots, V^i_D)$. The dimension of the upper limit and the lower limit of $\boldsymbol{V^i}$ (***Vmax*** and ***Vmin***) is also D. In the t-th iteration, the individual with the best fitness among all the individuals is $\boldsymbol{P^g}(t)$. For individual $\boldsymbol{x_i}$, up to the t-th iteration, the $\boldsymbol{x_i}$ with the best fitness is defined as $\boldsymbol{P^i}(t)$.

In each iteration, the velocity and location are updated as:

$$\begin{cases} V^i_j(t+1) = \omega V^i_j(t) + c_1 r_1[P^i_j(t) - X^i_j(t)] + c_2 r_2[P^g_j(t) - X^i_j(t)] \\ x^i_j(t+1) = x^i_j(t) + V^i_j(t+1) \end{cases} \tag{9}$$

where ω is the inertia weight value. c_1 and c_2 are called acceleration factors, which are non-negative values. r_1 and r_2 are random numbers in [0,1]. $V^i_j(t)$,$P^i_j(t)$ and $P^g_j(t)$ are the values of $\boldsymbol{V^i}(t)$,$\boldsymbol{P^i}(t)$ and $\boldsymbol{P^g}(t)$ in the j-th dimension respectively.

B. SSA

The salp swarm algorithm is to simulate the aggregation behavior of salps, which form a chain of salps and then hunt and move. The salp chain is made up of two types of salps: leaders and followers. The leaders are the salps at the head of the chain. Those slaps at the back of the chain are followers.

In the salp algorithm, food source F is defined as the individual with the best fitness among all individuals. The food source of the t-th order is $F(t)$.

Taking the minimization problem as an example, the process is shown in Fig. 5. The steps of the SSA algorithm are

1) Initialize the population. For all individuals, the positions are random numbers between the upper limit and the lower limit. Calculate the fitness of all individuals and sort them. The individual with the smallest fitness is the food source $F(t)$. t=1, because one iteration has been completed.

2) The population position is updated. The leader position is updated as:

$$x^i_j(t+1) = \begin{cases} F_j(t) + c_1[(ub_j - lb_j)c_2 + lb_j] & c_3 \geqslant 0.5 \\ F_j(t) - c_1[(ub_j - lb_j)c_2 + lb_j] & c_3 < 0.5 \end{cases} \tag{10}$$

where i=1, that is, the number of leaders is 1. It ranks first in the population. j=1,2$\cdots D$. $F_j(t)$, ub_j and lb_j are $F(t)$, ***ub,*** and ***lb*** in the j-th dimension respectively. c_2 and c_3 are random numbers in [0,1]. c_2 affects the step length of the leader's movement. c_3 determines whether the leader moves forward or backward to the food source. T is the maximum number of iterations. c_1 is the coefficient of the moving length. It is:

$$c_1 = 2e^{-(4t/T)^2} \tag{11}$$

The position of the follower is:

$$x^i_j(t+1) = 0.5(x^{i-1}_j(t) + x^i_j(t)) \tag{12}$$

where $i \geqslant 2$, and is the order of followers in the population. j=1,2$\cdots D$.

3) Calculate the fitness of all updated individuals. Sort the individuals. Update $F(t)$. Increase t by 1.

4) When the iteration accuracy requirement is reached or t=T, the iteration ends; otherwise, go to 2) to continue the iteration.

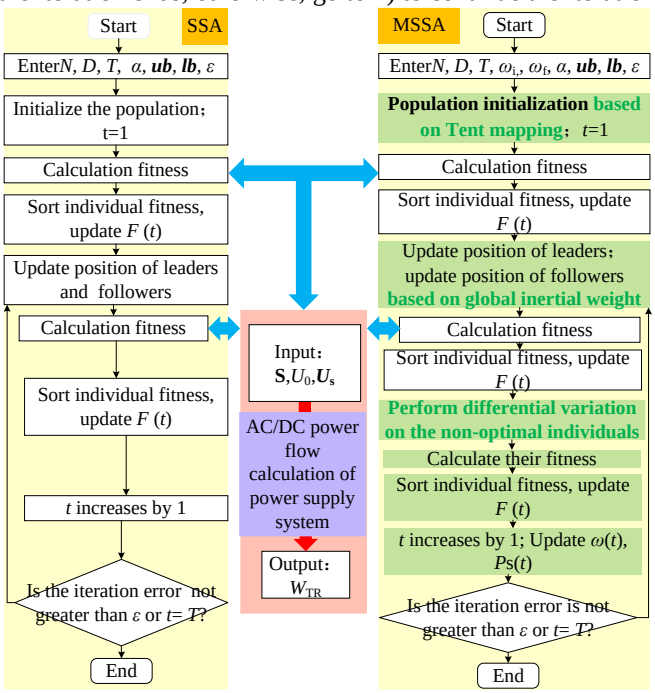

Fig. 5. Algorithm flow charts of SSA and MSSA.

C. MSSA

The improvements of MSSA include the following three aspects:

1) Tent chaos mapping

In the SSA, the initialization of the population is directly related to the efficiency of the algorithm. If the initialization of

the population is better, much iteration time can be saved. In SSA, the initialization of the population is achieved by random numbers.

The chaotic sequence has the characteristics of randomness, ergodicity, and regularity, and the salp populations produced by it have good diversity. The chaotic sequence generated by the Tent map is introduced to initialize the population. It is [21]:

$$\begin{cases} y_{j+1}^{i} = \begin{cases} \mu y_j^i, y_j^i < 0.5 \\ \mu(1-y_j^i), y_j^i \geqslant 0.5 \end{cases} \\ x_j^i(1) = (ub_j - lb_j)y_j^i + lb_j \end{cases} \tag{13}$$

where, $\mu \in (0,2]$, and is the chaotic parameter. The larger the μ is, the more chaos the system will be. It is set as 2. y^i_j is the chaotic sequence in [0,1].

2) Global inertial weight

The population success rate can be introduced as a feedback parameter to adaptively adjust the inertia weight factor [22]. From (12), it can be seen that the position of followers is only determined without considering the influence of the latter follower on the former follower and the changes in the fitness of the population. Therefore, the global inertial weight factor ω and the population success rate P_s are used to adaptively adjust the position of the followers. The P_s of the t-th iteration population, $P_s(t)$ is:

$$P_s(t) = \frac{1}{N}\sum_{i=1}^{N} S(i,t) \tag{14}$$

where $S(i,t)$ is the success value of individual $\boldsymbol{x^i}$. When the fitness of $\boldsymbol{x^i}(t)$ is better than the fitness of $\boldsymbol{P^i}(t)$, $S(i,t)=1$, otherwise $S(i,t)=0$. At the beginning of the iteration, the individuals are scattered and the exploration ability is strong. Therefore, the success value of the individual is mostly 1, and the success rate of the population $P_s(t)$ is also high. At the end of the iteration, the individuals of the population gradually gather, and the $P_s(t)$ gradually decreases. The position of followers is:

$$x_j^i(t+1) = 0.5(\omega(t)x_j^{i-1}(t) + x_j^i(t)) \tag{15}$$

where $\omega(t)$ is the global adaptive adjustment coefficient:

$$\omega(t) = \omega_i + (\omega_f - \omega_i)P_s(t)e^{-(\alpha t/T)^2} \tag{16}$$

where ω_i is the initial inertia weight coefficient. ω_f is the final inertia weight. α is the nonlinear control parameter.

3) Differential mutation

In the standard SSA algorithm, ignoring the mutation of non-optimal individuals may make it easy to fall into the local optimum during the process of the algorithm. The introduction of differential mutation can decrease the probability of local optimum [22]. The equation is:

$$x_j^i(t) = F_j(t) + \beta(x_j^{r1} - x_j^{r2}) \tag{17}$$

where β is the coefficient of mutation, which is 0.5. $r1$ and $r2$ are the serial numbers of any two individuals. $r1 \neq r2$. i is the serial number of the non-optimal individual. $i \neq r1$ and $i \neq r2$. If the fitness of the individual is worse than the fitness value of the individual before the mutation, the individual remains unchanged.

In this paper, half of the salp individuals are selected as the leaders to enhance the algorithm's global search ability and randomness in the early stage of the iteration. The process of MSSA proposed in this paper is as below and shown in Fig. 5.

1) Initialize the population. Enter N, D, T, ω_i, ω_f, α, $\boldsymbol{ub}$, $\boldsymbol{lb}$ and iteration precision ε. $P_s(1)=0$. Use Tent chaos mapping to generate initial values for all individuals. Calculate the fitness of all individuals and sort them. $F(t)$ is obtained. $t=1$.

2) The population position is updated. Update the position of the leader by (10). Update the position of the follower by (15).

3) Calculate the fitness of all updated individuals and sort them. Update $F(t)$.

4) Perform differential mutation by (7) for non-optimal individuals. Calculate fitness for all individuals after mutation, and retain individuals with better fitness.

5) Sort all individuals and update $F(t)$.

6) t is increased by 1. Update $\omega(t)$ and $P_s(t)$. When the iteration accuracy is no bigger than ε or $t=T$, the iteration ends; otherwise, go to 2) to continue the iteration.

D. Comparison of optimization methods

To compare the performance of these optimization algorithms using numerical tests, six benchmark functions are selected as in TABLE II. The dimension is the n in the functions. The range is the domain of x. The optimal values are all 0, which means that the closer to 0 the fitness value, the better.

PSO and SSA are used as control algorithms. Among the functions, $F_1(x)$~ $F_5(x)$ are single-peak functions，which are used to test the calculation accuracy and convergence speed of algorithms. $F_6(x)$ is a multi-peak function, which is used to test the global optimization ability of algorithms. In all algorithms, the population size is 30. The iteration number is 500. 30 independent simulation experiments are carried out to avoid the deviation caused by the randomness of the algorithm. Parameter selection is shown in TABLE III. The average values and standard deviations are calculated by the 30 independent experiments.

All simulations were run using a personal computer with an Intel(R) Core (TM) i9-9900K CPU @ 3.60 GHz and 12 GB of RAM. Numerical tests are carried out in Matlab.

TABLE II
BENCHMARK FUNCTIONS

Function	Dimension(n)	Range	Optimal value
$F_1(x) = \sum_{i=1}^{n} x_i^2$	30	[-100,100]	0
$F_2(x) = \sum_{i=1}^{n} \lvert x_i \rvert + \prod_{i=1}^{n} \lvert x_i \rvert$	10	[-10,10]	0
$F_3(x) = \sum_{i=1}^{n} \left(\sum_{j=1}^{i} x_j \right)^2$	10	[-100,100]	0
$F_4(x) = \max\{\lvert x_i \rvert, 1 \leq i \leq n\}$	10	[-100,100]	0
$F_5(x) = \sum_{i=1}^{n-1} [100(x_{i+1} - x_i^2)^2 + (x_i - 1)^2]$	10	[-30,30]	0
$F_6(x) = -20\exp(-0.2\sqrt{\frac{1}{n}\sum_{i=1}^{n} x_i^2}) - \exp(\frac{1}{n}\sum_{i=1}^{n}\cos(2\pi x_i)) + 20 + e$	10	[-20,20]	0

TABLE III
PARAMETER OF FUNCTIONS

Function	Parameter
PSO	ω=0.9； c_1=c_2=0.5
MSSA	ω_i=0.1, ω_f=0.9, α=0.09

The average value and standard deviation of the optimal value are calculated. The results of numerical tests are shown in TABLE IV. MSSA results are significantly better than PSO and SSA in both mean value and standard deviation, indicating that MSSA has a low degree of dispersion and good stability. Fig. 6. shows some convergence curves of three optimization algorithms. The convergence speed of MSSA is better than that of the other two algorithms.

TABLE IV
NUMERICAL TEST RESULTS

Function	Indicators	PSO	SSA	MSSA
$F_1(x)$	Average	0.1776	1.334E-07	1.865E-35
	Standard deviation	0.3375	1.741E-07	1.719E-35
$F_2(x)$	Average	0.6660	5.281E-05	2.135E-18
	Standard deviation	0.9314	1.317E-04	2.083E-18
$F_3(x)$	Average	3.195E-07	4.645E-07	6.486E-35
	Standard deviation	4.792E-07	8.380E-07	7.104E-35
$F_4(x)$	Average	1.206E-06	2.129E-05	4.717E-18
	Standard deviation	8.823E-07	4.123E-06	2.659E-18
$F_5(x)$	Average	6.458	13.771	6.909
	Standard deviation	9.107	18.567	0.267
$F_6(x)$	Average	2.382E-02	9.973E-03	6.930E-05
	Standard deviation	2.406E-02	3.735E-03	5.148E-05

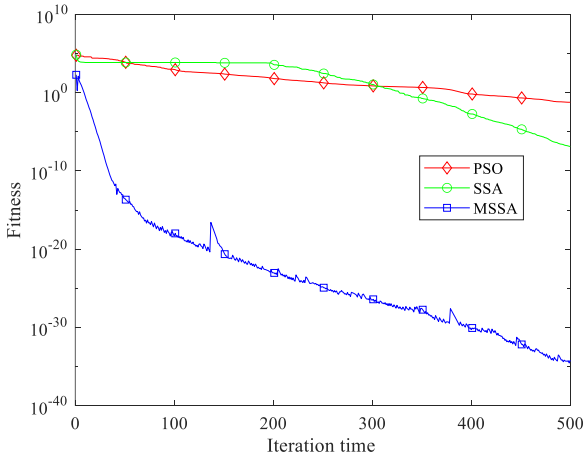

(a) $F_1(x)$

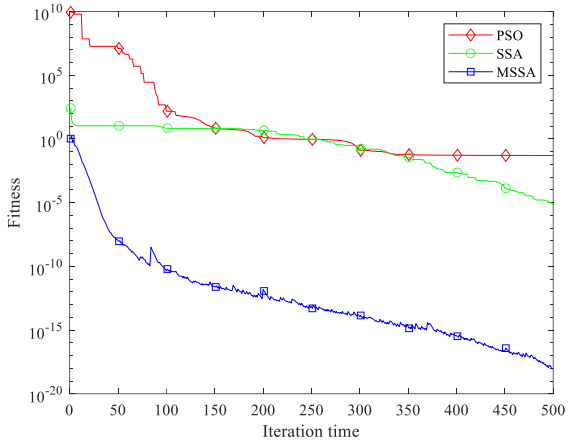

(b) $F_2(x)$

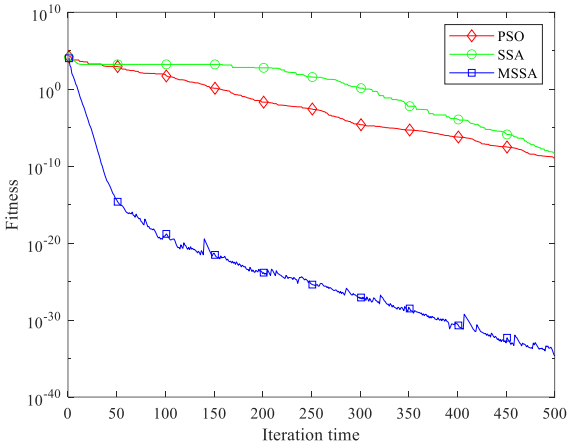

(c) $F_3(x)$

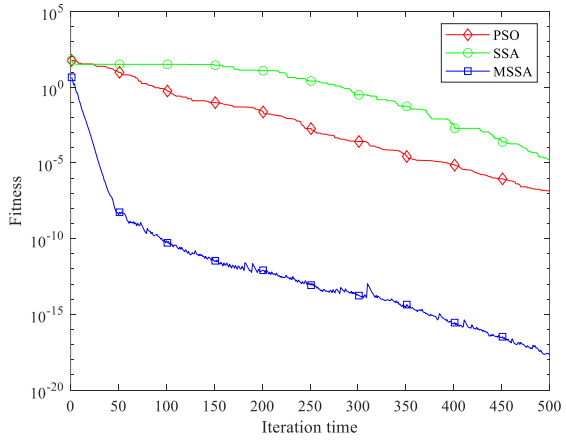

(d) $F_4(x)$

Fig. 6. Some convergent curves.

IV. CASE STUDY

A subway in Chengdu is taken as an example. The topology of the subway is shown in Fig. 7. It can reflect the actual geographic location of TSs and SSs. In Fig. 7., the number of the TS is T*i*. The number of the SS is S*i*. The train operation curves are shown in Fig. 8. Parameters of the subway line are shown in TABLE V. The substation positions are shown in TABLE VI. The abovementioned parameters and figures are the input of later simulations.

The subway simulation software is DCTPS, which is developed by the authors' research group. It was written in

C++. And the AI algorithms are added into DCTPS to carry out subway simulations.

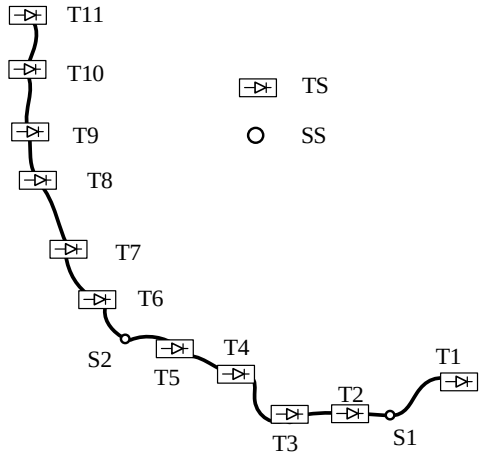

Fig. 7. Topology of the subway in Chengdu.

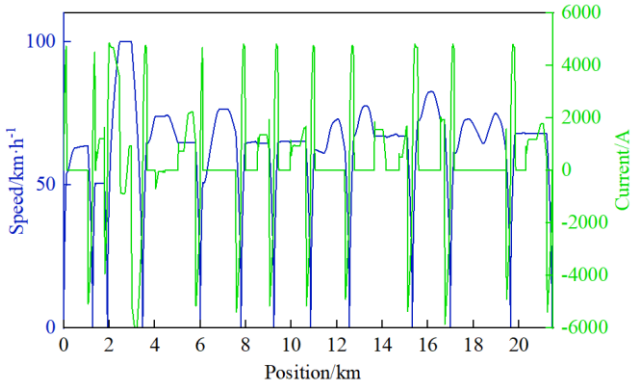

(a) Course from T1 to T11

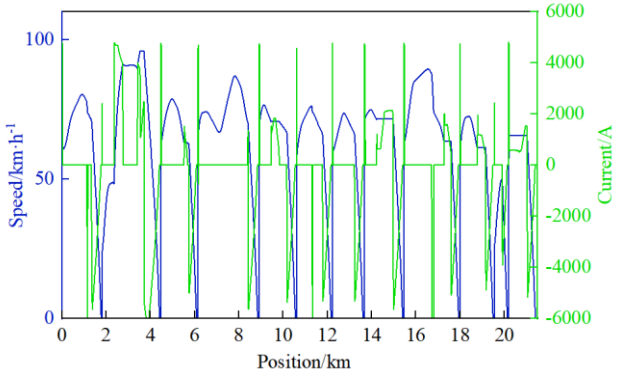

(b) Course from T11 to T1

Fig. 8. Train operation curves.

TABLE V
PARAMETERS OF THE SUBWAY LINE

Simulation parameter	Value
Rectifier unit rated power	3.6MW
Contact network resistance	0.0172Ω/km
Rail resistance [31][32]	0.02Ω/km
Rail-earth resistance	15Ωkm
Maximum train speed	100km/h
Train weight	462t

TABLE VI
SUBSTATION POSITIONS OF THE SUBWAY IN SHENZHEN

Station	Position (km)	Station	Position (km)
T1	0.451	T6	11.304
S1	1.717	T7	13.006
T2	2.367	T8	15.772
T3	3.920	T9	17.442
T4	6.452	T10	20.082
T5	8.246	T11	21.909
S2	9.688		

A. *Impact factors of STEC*

To study the impact factors of STEC, U_0 and U_s are chosen as parameters. W_{TR} under different U_s and U_0 is shown in Fig. 9, where ε_{U_0} is [1600V, 1680V], ε_{U_s} is [1700V, 1760V]. The results are based on simulation. When U_0 is unchanged, W_{TR} and U_s are positively correlated. When U_s is constant, W_{TR} and U_0 show an overall positive correlation trend, but they are not completely positively correlated.

It can be derived from (2) and (3) that W_{TR} is:

$$W_{TR}=\frac{1}{\eta_T}W_{trac}-\eta_F W_{reg}+(\frac{1}{\eta_T}-\eta_F)W_{reg\text{-}trac}+\eta_F W_{res}+\eta_F W_{loss1}+\frac{1}{\eta_T}W_{loss2}+W_R \tag{18}$$

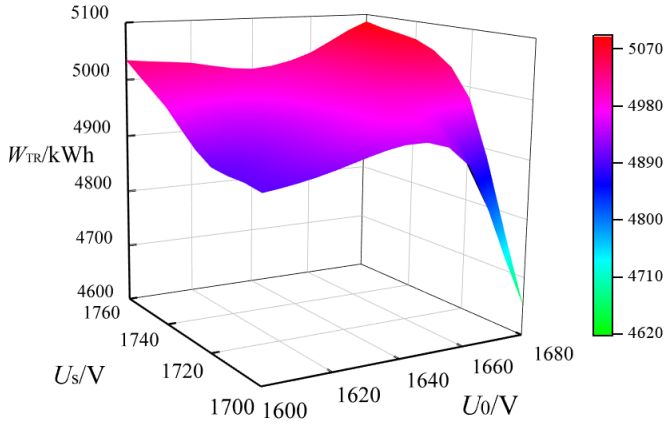

Fig. 9. W_{TR} under different U_s and U_0

When the train operation timetable remains unchanged, both W_{trac} and W_{reg} remain unchanged. η_T should be higher than 0.98 and η_F should be higher than 0.95 so the coefficient of $W_{reg\text{-}trac}$ is small and this item can be ignored.

When U_0 remains unchanged and U_s increases, the operation time of EFSs decreases and the feedback power decreases. W_R may decrease. Since EFS also has the function of controlling the TN voltage, the decrease of the operation time of EFSs means the TN voltage increases. W_{res} will increase and (W_{loss1}+ W_{loss2}) will decrease. The results in Fig. 9. show that when U_s increases from 1750V to 1780V, the increase of W_{res} is greater than the decrease in W_R and (W_{loss1}+ W_{loss2}), so W_{TR} increases.

When U_s remains unchanged and U_0 increases, the TN voltage increases and the difference between U_s and U_0 decreases, so EFSs start more. The increase of feedback energy means that W_R may increase, and on-board braking resistors are also easier to start, and W_{res} will increase. The current required

to transmit the same power becomes smaller, and (W_{loss1}+ W_{loss2}) will decrease. Fig. 9. shows that when U_0 increases from 1600V to 1700V, W_{TR} shows an overall increasing trend. However, the W_{TR} of 1620V is less than the W_{TR} of 1600V, indicating that the decrease in (W_{loss1}+ W_{loss2}) is greater than the increase in W_R and W_{res}.

The above analysis shows that when the U_s is unified for the entire line in [1750V, 1780V], the lower the U_s is, the smaller the W_{TR} is. Due to the uneven distribution of regenerative braking energy across the line, independent optimizing U_s for each EFS is necessary. U_0 should not be as low as possible. Since the adjustment of U_0 is generally achieved by adjusting the transformer tap, it is hard for each TS to adjust U_0. Therefore, U_0 should be selected as a unified parameter for optimization.

B. Optimal Parameter design

Except for parameters in TABLE V, other simulation parameters are shown in TABLE VII. The operation timetable of trains is shown in TABLE VIII, where the initial stage of the operation is 3 years. The recent stage of the operation is 7 years.

TABLE VII
PARAMETERS OF SIMULATION

Simulation parameter	Value	Simulation parameter	Value
EFS life span	10 year	U_{rmax}	120V
c_{mt}	¥1000 RMB/year	U_{tmax}	1800V
r	1.02	U_{tmin}	1000V
ε_S	{0.5x |x=0,1,2,3,4,5,6} (MW)	E_y	¥0.75 RMB/kWh

TABLE VIII
OPERATION TIMETABLE OF TRAINS

Departure interval	Daily duration in initial stage/h	Daily duration in recent stage/h
8 pairs/h	14	3
10 pairs/h	4	11
16 pairs/h	0	4

There are five schemes: RS, SSA, PSO, MSSA Case1, MSSA Case2. To verify the energy-saving and investment-saving effects of EFS, the RS is set as a control group, and U_0 is 1660V. Simulations with SSA and PSO are also control groups to compare different algorithms, and the parameters are S, U_0, and U_s. According to the analysis of section A, U_0 and U_s should be optimization parameters. To verify it, experiments applying MSSA with only S as the optimization variable is carried out. It is defined as MSSA Case1. In MSSA Case1, U_s is 1720V. U_0 is 1660V. MSSA with U_s, U_0, and S as optimization variables is defined as MSSA Case2.

The iteration processes are shown in Fig. 10. Due to the introduction of Tent chaos mapping, the initial value of MSSA Case1 decreases by 0.39% and 0.55% respectively compared with that of PSO and SSA. The initial value of MSSA Case2 decreases by 0.58% and 0.74%.

The evolution rate of MSSA Case2 is faster than MSSA Case1, which proves the necessity of U_S and U_0 as optimization variables.

After 16 generations, the evolution of SSA halts. After 5 generations, the evolution of PSO halts. However, after 39 generations, MSSA can still evolve, which indicates that the introduction of global inertia weight and difference of mutation can significantly improve the evolution of the algorithm in the later iteration.

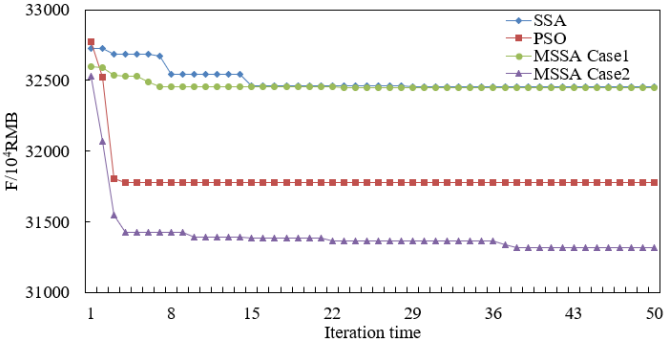

Fig. 10. Iteration process.

The final objective function values and sub-objective function values of the five schemes are shown in TABLE IX. Compared to the RS, MSSA Case2 can save composite cost by 29.47%when EFSs reach the life span. Compared with PSO, SSA, and MSSA Case1, the composite cost of MSSA Case2 is 1.43%, 3.50%, and 3.49% less, respectively.

TABLE IX
PARAMETER OPTIMIZATION CONFIGURATION RESULTS

Scheme	f_1(**S**) / 10^6 RMB	f_2(**S**, U_0, **U_s**) / 10^6 RMB	F(**S**, U_0, **U_s**) / 10^6 RMB
RS	0	444.04	444.04 (100%)
PSO	15.80	301.93	317.74 (72%)
SSA	10.41	314.13	324.54 (73%)
MSSA Case1	11.52	312.96	324.49 (73%)
MSSA Case2	11.52	301.65	313.17 (71%)

The final parameter configurations of the four schemes are shown in TABLE X. The results of PSO and MSSA Case2 are compared. The distance between T3-T4, T7-T8, and T9-T10 of this line is relatively large. In these sections, there is less chance for the adjacent vehicles to absorb regenerative braking energy. Therefore, EFSs can absorb regenerative braking energy more effectively. The TN voltage can be better controlled. The energy-consuming of on-board braking resistance decreases, so a better energy-saving effect is achieved. As can be seen from TABLE X, MSSA Case2 sets EFSs at T2, T5, T6, T8, T9, and T10. The suboptimal solution of the four optimization schemes, PSO, sets EFS at T1, T2, T3, T7, T8, and T9. Since the station spacing between T1-T3 is not the maximum, EFS in T1, T2, and T3 will increase the investment cost of the system while the energy-saving effect will be limited. As can be seen from TABLE IX, although the $\boldsymbol{f_2(S, U_0, U_s)}$ of PSO is close to that of MSSA, the $\boldsymbol{f_1(S)}$ of PSO is 37.12% larger than that of MSSA.

The results of MSSA Case1 and MSSA Case2 are also compared. The $\boldsymbol{f_1(S)}$ of MSSA Case1 is the same as the $\boldsymbol{f_1(S)}$ of MSSA Case2. In MSSA Case1, EFSs are set at T1, T2, T4, T5, T8, and T11. There are two more EFSs than MSSA Case2 in the T1~ T5 section. It indicates that when U_S and U_0 are set as the unit values, regenerative braking energy can be feedback by EFS more effectively. In MSSA Case2, the EFS rated power of T10 is 1.5MW and its U_S is 1750V. In the section where the EFSs are set continually, a slightly higher U_S can be configured to share the regenerative braking energy with other adjacent

EFSs.

TABLE X
FINAL PARAMETER CONFIGURATIONS OF THE FOUR SCHEMES

Scheme	PSO			SSA			MSSA Case1			MSSACase2		
	S/MW	U_0/V	U_s/V	*S*/MW	U_0/V	U_s/V	*S*/MW	U_0/V	U_s/V	*S*/MW	U_0/V	U_s/V
T1	3		1700	0		-	1.5			0		-
T2	3		1700	3		1760	2			3		1700
T3	3		1700	0		-	0			0		-
T4	0		-	0		-	2			0		-
T5	0		-	2.5		1760	3			2		1700
T6	0	1680	-	1.5	1680	-	0	1660	1720	1	1680	1700
T7	3		1700	3		1760	0			0		-
T8	3		1700	0		-	2			2.5		1700
T9	3		1750	2.5		1760	0			3		1700
T10	2		1700	0		-	0			1.5		1750
T11	0		-	0		-	2.5			0		-

V. CONCLUSION

In this paper, the energy audit index is proposed, and the parameter designing model for power supply system in urban rail which takes the composite cost of the system as the object when the life span of EFSs reaches is built. MSSA is proposed for the solution of the model. Here are the conclusions:

1) The STEC can reflect the system-level energy consumption level and avoid the influence of the fluctuation of step-down loads through a field test.

2) MSSA has a faster convergence speed than SSA and PSO in the numerical experiments and the actual subway project. Compared with the reference system without EFS, MSSA can save 29.47% of the overall cost when EFS reaches its life period. Compared with PSO, SSA, the comprehensive cost of MSSA can be saved by 1.43%, 3.50%, respectively.

3) The start voltage of EFS and no-load voltage should also be taken into account when designing system parameters. The composite cost of MSSA which takes EFS rated power, start voltage and no-load voltage of rectifier units as optimization parameters is 3.49% less than the composite cost of MSSA which only takes EFS rated power as the optimization parameter.

REFERENCES

[1] J. Chen, H. Hu, Y. Ge, K. Wang, W. Huang, and Z. He, "An energy storage system for recycling regenerative braking energy in high-speed railway," *IEEE Trans. Power Delivery*, vol. 36, no. 1, pp. 320-330, Feb. 2021.

[2] J. Zhang, W. Liu, Z. Tian, H. Zhang, J. Zeng, H. Qi, "Modelling, simulating and parameter designing for traction power system with bidirectional converter devices," *IET Generation, Transmission & Distribution*, vol. 16, no. 1, pp. 110-122. Aug 2021.

[3] Z. Tian, S. Hillmansen, C. Roberts, P. Weston, N. Zhao, L. Chen, and M. Chen, "Energy evaluation of the power network of a DC railway system with regenerating train," *IET Electrical Systems in Transportation*, vol. 6, no. 2, pp. 41-49, Jun. 2016.

[4] A. Higuera, A. Claudio, L. Vela, L. Hernandez, and J. Valdez, "Energy Performance Analysis In An Electrical Subway Traction System, " *IEEE Latin America Transactions*, vol. 14, no. 2, pp. 729-736, Feb. 2016.

[5] L.Alfieri, L.Battistelli, and M.Pagano, "Energy efficiency strategies for railway application: alternative solutions applied to a real case study, " *IET Electr. Syst. Transp.*, vol. 8, no. 2, pp. 122-129. Jun. 2018.

[6] H. Hayashiya et al., "Evaluation of energy saving effect of traction power supply voltage in urban electric railway system, " in *EPE'18 ECCE Europe*, Riga, Latvia, 2018.

[7] M. Özcan, S. Açıkbaş, S. Boynukalın, M. Söylemez, "Effect of station heights on energy efficiency in a metro line using regenerative braking, " in *11th ELECO*, Bursa, Turkey, 2019, pp. 825-829.

[8] K. Wang, H. Hu, J. Chen, J. Zhu, X. Zhong, and Z. He, "System-Level Dynamic Energy Consumption Evaluation for High-Speed Railway," *IEEE Transactions on Transportation Electrification*, vol. 5, no. 3, pp. 745-757, Sept. 2019.

[9] W. Liu, J. Zhang, H. Wang, T. Wu, Y. Lou, X. Ye, "Modified AC/DC unified power flow and energy-saving evaluation for urban rail power supply system with energy feedback systems," *IEEE Transactions on Vehicular Technology*, vol. 70, no. 10, pp. 9898-909, Oct. 2021.

[10] Z. Tian, G. Zhang, N. Zhao, S. Hillmansen, P. Tricoli, and C. Roberts, "Energy evaluation for DC railway systems with inverting substations," in *ESARS-ITEC*, Nottingham, 2018, pp. 1-6.

[11] M. Dominguez, A. Fernández-Cardador, A. P. Cucala, and R. R. Pecharroman, "Energy Savings in Metropolitan Railway Substations Through Regenerative Energy Recovery and Optimal Design of ATO Speed Profiles," *IEEE Transactions on Automation Science and Engineering*, vol. 9, no. 3, pp. 496-504, Jul. 2012.

[12] A. González-Gil, R. Palacin, P. Batty, and J.P. Powell, "A systems approach to reduce urban rail energy consumption," *Energy Conversion and Management*, vol. 80, pp. 509-524, Apr. 2014.

[13] V. A. Kleftakis and N. D. Hatziargyriou, "Optimal Control of Reversible Substations and Wayside Storage Devices for Voltage Stabilization and Energy Savings in Metro Railway Networks," *IEEE Transactions on Transportation Electrification*, vol. 5, no. 2, pp. 515-523, June 2019.

[14] S. Lian, "A rated power allocation method of regenerative energy feedback device suitable for multi-train running scenarios in urban rail transit," *Railway Standard Design*, vol. 62, no. 9, pp. 149-154+186, Sep. 2018.

[15] W. Jefimowski and A. Szelag, "The multi-criteria optimization method for implementation of a regenerative inverter in a 3 kV DC traction system," *Electric Power Systems Research*, vol. 161, pp. 61-73, Aug. 2018.

[16] L. Tan, J. Han, and H. Zhang, "Ultra-Short-Term Wind Power Prediction by Salp Swarm Algorithm-Based Optimizing Extreme Learning Machine," *IEEE Access*, vol. 8, pp. 44470-44484, 2020.

[17] A. M. Shaheen and R. A. El-Sehiemy, "A Multiobjective Salp Optimization Algorithm for Techno-Economic-Based Performance Enhancement of Distribution Networks," *IEEE Systems Journal*, vol. 15, no. 1, pp. 1458-1466, March 2021.

[18] A. J. Lopez-Lopez, R. R. Pecharroman, A. P. Cucala, and A. Fernandez-Cardador, "Optimizing mass transit systems electrical infrastructure by application of the particle swarm optimization algorithm," in *VPPC*, Hanoi, Vietnam, 2019.

[19] S. Mirjalili, A. H. Gandomi, S. Z. Mirjalili, S. Saremi, H. Faris, and S. M. Mirjalili, "Salp swarm algorithm: A bio-inspired optimizer for engineering design problems," *Advances in Engineering Software*, vol. 114, no. 6, pp. 163-191, Jul. 2017.

[20] D. H. Wolpert and W. G. Macready, “No free lunch theorems for optimization,” *IEEE Trans on Evolutionary Computation*, vol. 1, no. 1, pp. 67-82, Apr. 1997.
[21] D. Zhang, Z. Chen, Z. Xin, H. Zhang, and W. Yan, “Salp swarm algorithm based on craziness and adaptive,” *Control and Decision*, vol. 35, no. 9, Sep. 2020.
[22] Y. Bai and Z. Peng. Salp swarm algorithm based on adaptive inertia weight. *Control and Decision*. [Online]. Available: https://doi.org/10.13195/j.kzyjc.2020.0454.
[23] R. Wang, Y. Li, J. Fan, T. Wang, and X. Chen, “A Novel Pure Pursuit Algorithm for Autonomous Vehicles Based on Salp Swarm Algorithm and Velocity Controller, ” *IEEE Access*, vol. 8, pp. 166525-166540, Sep. 2020.
[24] B. Ma, H. Ni, X. Zhu, and R. Zhao, “A Comprehensive Improved Salp Swarm Algorithm on Redundant Container Deployment Problem, ” *IEEE Access*, vol. 7, pp. 136452-136470, Oct. 2019.
[25] L. Zhang, C. Li, Y. Wu, J. Huang, and Z. Cui, “An Improved Salp Swarm Algorithm With Spiral Flight Search for Optimizing Hybrid Active Power Filters’ Parameters, ” *IEEE Access*, vol. 8, pp. 154816-154832, Sep. 2020.
[26] J. Zhang and J. S. Wang, “Improved Salp Swarm Algorithm Based on Levy Flight and Sine Cosine Operator, ” *IEEE Access*, vol. 8, pp. 99740-99771, Jun. 2020.
[27] R. M. Rizk-Allah and A. E. Hassanien, “Locomotion-based Hybrid Salp Swarm Algorithm for Parameter Estimation of Fuzzy Representation-based Photovoltaic Modules, ” *Journal of Modern Power Systems and Clean Energy*, vol. 9, no. 2, pp. 384-394, Mar. 2021.
[28] O. H. Ahmed, J. Lu, A. M. Ahmed, A. M. Rahmani, M. Hosseinzadeh, and M. Masdari, “Scheduling of Scientific Workflows in Multi-Fog Environments Using Markov Models and a Hybrid Salp Swarm Algorithm, ” *IEEE Access*, vol. 8, pp. 189404-189422, Oct. 2020.
[29] R. Chen, C. Dong, Y. Ye, Z. Chen, and Y. Liu, “QSSA: Quantum Evolutionary Salp Swarm Algorithm for Mechanical Design, ” *IEEE Access*, vol. 7, pp. 145582-145595, Oct. 2019.
[30] X. Zhao, F. Yang, Y. Han, and Y. Cui, “An Opposition-Based Chaotic Salp Swarm Algorithm for Global Optimization,” *IEEE Access*, vol. 8, pp. 36485-36501, Mar. 2020.
[31] A. Wang, S. Lin, Z. Hu, J. Li, F. Wang, G. Wu, and Z. He, “Evaluation Model of DC Current Distribution in AC Power Systems Caused by Stray Current of DC Metro Systems,” *IEEE Trans on Power Delivery*, vol. 36, no. 1, pp. 114-123, Feb. 2021.
[32] S. Lin, A. Wang, M. Liu, X. Lin, Q. Zhou, and L. Zhao, “A Multiple Section Model of Stray Current of DC Metro Systems,” *IEEE Trans on Power Delivery*, vol. 36, no. 3, pp. 1582-1593, June 2021.

Jian Zhang received the B.S. degree in Electrical Engineering from Southwest Jiaotong University, Chengdu, China, in 2017. He is currently working toward a Ph.D. degree in Southwest Jiaotong University, Chengdu, China.

His research interest includes regenerative braking energy utilizing in the power supply system of urban rail transit.

Wei Liu received the B.S., M.S., and Ph. D degrees in Electrical Engineering from Southwest Jiaotong University, Chengdu, China, in 2003, 2006, and 2009, respectively.

He is currently an associate professor in the School of Electrical Engineering at Southwest Jiaotong University, Chengdu, China. His research interests include theoretical and simulation research of traction power supply system of urban rail, regenerative braking energy utilization, the theory, and control research of stray current and rail potential.

Zhongbei Tian received the B.Eng in Huazhong University of Science and Technology, Wuhan, China, in 2013. He received the B.Eng. and Ph.D. degree in Electrical and Electronic Engineering from the University of Birmingham, Birmingham, U.K., in 2013 and 2017. He is currently a Lecturer in Electrical Energy Systems at the University of Liverpool. His research interests include railway traction power system modeling and analysis, energy-efficient train control, energy system optimization, and sustainable transport energy systems integration and management.

He Qi received the B.S. degree in Electrical Engineering from Taiyuan University of Technology, Taiyuan, China, in 2020. He is currently working toward an M.S. degree in Southwest Jiaotong University, Chengdu, China.

His research interest includes system modeling in the power supply system of urban rail transit.

Jiaxin Zeng received the B.S. degree in Rail Traffic Signaling and Control from Xihua University, Chengdu, China, in 2020. She is currently working toward an M.S. degree in Southwest Jiaotong University, Chengdu, China.

Her research interest includes bidirectional converter systems in the power supply system of urban rail transit.

Yuheng Yang received the B.S. degree in Electrical Engineering from Panzhihua University, Panzhihua, China, in 2020. He is currently working toward an M.S. degree in Southwest Jiaotong University, Chengdu, China.

His research interest includes energy storage system in power supply system of urban rail transit.